Role of changes in mean temperatures vs. temperature gradients in the recent widening of the Hadley circulation

Ori Adam[1*], Tapio Schneider[1, 3] and Nili Harnik[2]

[1] Department of Earth Sciences, ETH Zürich, 8092 Zürich, Switzerland.

[2] Department of Geophysical, Atmospheric and Planetary Sciences, Tel-Aviv University, Israel.

[3] California Institute of Technology, Pasadena, CA, USA

17-Feb-14

[*]Corresponding author. Email: ori.adam@live.com

JOC, In Preparation

Abstract

The Hadley circulation (HC) has widened substantially in recent decades, and it widens as the climate warms in simulations. But the mechanisms responsible for the widening remain unclear, and the widening in simulations is generally smaller than observed.

To identify mechanisms responsible for the HC widening and for model-observation discrepancies, this study analyzes how interannual variations of tropical mean temperatures and meridional temperature gradients influence the HC width. Changes in mean temperatures are part of any global warming signal, whereas changes in temperature gradients are primarily associated with ENSO. Six reanalysis datasets, 22 Atmospheric Modeling Intercomparison Project (AMIP) simulations, and 11 historical Climate Modeling Intercomparison Project Phase 5 (CMIP5) simulations are analyzed, covering the years 1979-2012. The HC widens as mean temperatures increase or as temperature gradients weaken in most reanalyses and climate models. On average, climate models exhibit a smaller sensitivity of HC width to changes in mean temperatures and temperature gradients than reanalyses. However, the sensitivities differ substantially among reanalyses, rendering the HC response to mean temperatures in climate models not statistically different from that in reanalyses.

While global-mean temperatures did not increase substantially between 1997 and 2012, the HC continued to widen in most reanalyses. The analysis here suggests that the HC widening from 1979 to 1997 is primarily the result of global warming, whereas the widening of the HC from 1997 to 2012 is associated with increased midlatitude temperatures and hence reduced temperature gradients during this period.

1. Introduction

The Hadley circulation (HC) has widened in recent decades, leading to an expansion of the subtropical dry zones (Hu and Fu 2007; Johanson and Fu 2009; Seidel and Randel 2007; Lucas et al. 2014; Cubasch et al. 2013; Nguyen et al. 2013). Climate models of Phase 3 (Johanson and Fu 2009) and Phase 5 (Ceppi and Hartmann 2012) of the Climate Model Intercomparison Project (CMIP3 and CMIP5) underestimate the widening, which has led to speculations about the reliability of models and reanalyses (Johanson and Fu 2009; Quan et al. 2013) and of HC extent diagnostics (Davis and Rosenlof 2012).

The relative roles of global warming and of other climate variations in the recent widening of the HC are unclear. In idealized and comprehensive climate simulations, the total HC width (HCW, defined as the latitudinal distance between the northern and southern termini of the HC) increases on average by ~1.2 degree latitude per Kelvin global surface temperature increase (º/K) (Lu et al. 2007). Yet, observations indicate that the HCW has increased at a substantially larger rate of up to ~7 º/K (depending on the reanalysis used and the definition of HCW) between 1979 and 2005 (Johanson and Fu 2009). Additionally, global warming—indicated by the positive trend in global mean surface temperature—appears to have 'paused' between 1997-2012 (Cubasch et al. 2013), yet here we show that the widening of the HC has continued during that time.

The goal of the present paper is to identify factors that play a role in the observed and simulated widening of the HC and to assess their relative importance in observations and models, so that possible causes of model biases can be pinpointed.

Starting from the observation that El Niño and the Southern Oscillation (ENSO) are associated with substantial changes in HCW—the HC narrows during El Niño and widens during La Niña (Seager et al. 2003; Nguyen et al. 2013)—we define simple indices that decompose sea surface temperature (SST) variations orthogonally into factors that are primarily associated with global warming (mean SST changes) and ENSO (SST gradient changes).

We compare interannual variability and trends of the Hadley circulation width in 6 reanalysis datasets with 22 Atmospheric Model Intercomparison Project (AMIP) simulations, in which atmospheric GCMs are driven by prescribed historical SST, and with 11 CMIP5 historical simulations, in which coupled ocean-atmosphere GCMs are driven by prescribed historical atmospheric compositions (e.g., greenhouse gases and volcanic aerosols). This allows us to separate HCW trends owing to different factors: effects of recent changes in atmospheric composition, which should be captured in both AMIP and CMIP5 simulations, can be separated from the effects of recent changes in ocean conditions not related to external forcings (e.g., ENSO), which would be captured in AMIP but not necessarily in CMIP5 simulations.

2. Data

Annual mean data derived from monthly means for the years 1979-2012 were analyzed from the 6 reanalysis datasets listed in Table 1 (with the exception of the 20th Century Reanalysis, for which only data through 2011 were available). Sea surface temperature and the Oceanic Niño Index (ONI, the deviation of the 3-month running mean SST from a moving 30-year climatology in the Nino 3.4 region) were obtained from the Extended Reconstructed SST (ERSST v3b) provided by the National Oceanic and Atmospheric Administration's National Climatic Data Center (Smith et al. 2008). Global surface temperature anomalies were obtained from the National Aeronautics and Space Administration's Goddard Institute for Space Studies GISTEMP (Hansen and Lebedeff, 1987), in which ERSST v3b is used for SST anomalies.

CMIP5 and AMIP monthly simulation data were downloaded from the Earth System Grid Federation (ESGF). A total of 22 AMIP and 11 CMIP5 simulations are used, covering the periods 1979-2008 and 1979-2005, respectively. Only the first ensemble run is analyzed for each model simulation. Model names, affiliations, and spatial resolutions are listed in Table 1. Additional information is available at the CMIP website http://cmip-pcmdi.llnl.gov.

3. Results

The dominant interannual SST variations are associated with global warming and ENSO. Figure 1a shows the first (solid red) and second (solid blue) EOF of zonally averaged interannual SST variations around their long-term mean for the years 1979-2012. (For the principal component analysis, annual- and zonal-mean SSTs are computed from monthly SST variations around their long-term monthly mean, and variances and covariances are area-weighted.) The associated principal components account for 42% and 25% of the variance of the annual- and zonal-mean SSTs (Fig. 1b), respectively. It is evident from the structure of the EOFs and the principal component time series that the first EOF represents a global-warming signal and the second is associated with ENSO. Indeed, the SST difference between typical El Niño and La Niña conditions resembles the second EOF (Fig. 1a), and the associated principal component time series correlates strongly with ONI (Fig. 1b). The principal way in which ENSO variations manifest themselves in SST are changes in the meridional SST contrast between the tropics and midlatitudes.

The dominant interannual SST variations motivate a decomposition of SST variations into two simple orthogonal components, one associated with large-scale temperature changes and one associated with changes in meridional temperature contrasts between the tropics and midlatitudes. We define the indices *Mean(SST)* and *Grad(SST)* as the area-weighted mean SST anomaly between ±45° (total shaded area in Fig. 1a) and the difference between the mean SST anomaly between 20-45° in both hemispheres (dark shaded area) and the mean SST anomaly between ±20° (light shaded area). This choice of latitude belts is motivated by the structure of the second (ENSO) EOF, showing contrasting SST variations between ±20° and midlatitudes. The 0-20° and 20-45° latitude belts are approximately of equal area, making *Mean(SST)* and *Grad(SST)* orthogonal. Note that our choice of signs implies that *Grad(SST)* increases (becomes less negative) when midlatitudes warm differentially relative to the tropics, so that it is negative during El Niño and positive during La Niña. The advantage of this sign convention is that HCW then is expected to increase as either *Mean(SST)* or *Grad(SST)* increase, implying positive sensitivities of HCW with respect to either index.

Figure 2 shows the time series of annually averaged *Mean(SST)* (top, solid green) and *Grad(SST)* (bottom, solid blue) for the years 1979-2012. The trends of these indices during the periods 1979-1997 and 1997-2012 are shown by solid gray lines with gray shadings marking Studentized 95% confidence bounds. The global-mean surface temperature anomaly (dashed magenta; GISTEMP) for the same period and latitude belt as *Mean(SST)* is shown for reference in the top panel. It is clear that *Mean(SST)* correlates strongly with global-mean SST variations, but the inclusion of land areas in the global-mean SST variations increases their variance. The ONI (dashed orange, multiplied by -1) is shown for reference in the bottom panel. As expected, *Grad(SST)* correlates strongly with ONI, with a (Pearson) correlation coefficient of -0.8.

To establish how the SST variations relate to HC variations, we define the terminus of the HC as the first latitude where the meridional mass stream function, averaged between the 850 and 300 hPa levels, changes sign poleward of the tropical extrema. The vertical averaging of the stream function reduces sensitivity to vertical structure (Kang et al. 2013; Davis and Birner 2013). The resulting HCW (latitudinal distance between the northern and southern termini of the HC) has relatively small inter-model variability (e.g., Johanson and Fu 2009; Quan et al. 2013; Nguyen et al. 2013) and is generally consistent with other, similar extent indices (Davis and Rosenlof 2012).

The top panel of Figure 3 shows the time series of the annual-mean HCW from the 6 reanalyses for the years 1979-2011. The northern and southern HC termini are shown separately in the bottom panel. The HC widening is predominantly due to the poleward migration of the HC terminus in the northern hemisphere (Hu and Fu 2007), where the latitude of the terminus is also more variable than in the southern hemisphere. The standard deviation of the spread of HCW's across the reanalyses is 0.2°, increasing with time at a statistically significant ($p<0.05$) rate of 30% per decade.

Figure 4 shows trends in HC extent in the southern hemisphere (left column) and northern hemisphere (right column) over the years 1979-2005 for the 6 reanalyses (orange triangles), for the 22 AMIP simulations (blue crosses), and for the 11 CMIP5 simulations (green dots) listed in Table 1. Error bars mark Studentized 95% confidence bounds. Ensemble means over reanalyses and simulations are shown without error bars. The spread in trends across reanalyses is much higher than that across models both in AMIP and CMIP5 simulations (Quan et al. 2012).

We calculate the sensitivity of HCW to variations in *Mean(SST)* and *Grad(SST)* for each simulation by linearly regressing HCW against the SST indices. The regression analysis is restricted to annual means, so that any sub-annual lag between SST variations and the HC does not affect the results (Kang and Lu 2012; Davis and Birner 2013). The regression model is

$$\mathrm{HCW} = a_0 + a_1 \cdot Mean(SST) + a_2 \cdot Grad(SST) + \varepsilon$$

where the coefficients a_1 and a_2 represent the sensitivity of the HCW to variations in *Mean(SST)* and *Grad(SST)*, a_0 is an intercept, and ε a residual.

Figure 5 shows the sensitivities for each reanalysis and simulation (with error bars marking Studentized 95% confidence bounds), calculated using the longest available period in each dataset (1979-2012 for reanalyses, orange triangles; 1979-2008 for AMIP simulations, blue crosses; and 1979-2005 for CMIP5 simulations, green dots). These sensitivities do not change substantially if the period of overlap among the datasets, 1979-2005, is used for AMIP simulations and reanalyses.

The sensitivities to *Mean(SST)* vary considerably across reanalyses. The NCEP I, NCEP II and 20C reanalyses show statistically significant ($p<0.05$) positive sensitivities, indicating that the HC widens as *Mean(SST)* increases. By contrast, ERA-Interim, CFSR, and MERRA show no statistically significant sensitivity to *Mean(SST)*. Most climate simulations exhibit a sensitivity to *Mean(SST)* similar to that found for the ERA-Interim, CFSR, and MERRA reanalyses, with only 4 of the 33 AMIP and CMIP simulations showing a statistically significant positive sensitivity to *Mean(SST)*.

All reanalyses exhibit a statistically significant positive sensitivity to *Grad(SST)*. Similarly, 26 of the 33 climate simulations show a statistically significant positive sensitivity to *Grad(SST)*. On average, the sensitivities of the ERA-Interim, CFSR, and MERRA reanalyses (~4.5°/decade) are smaller than those found for the NCEP I, NCEP II, and 20C reanalyses (~8.5°/decade), and are closer to those found in the AMIP and CMIP5 simulations (~3°/decade).

Figure 6 shows the relative contributions of *Mean(SST)* (green) and *Grad(SST)* (blue) to the observed HCW changes (orange) during the entire period over which reliable data are available (1979-2012, Fig. 6a) and restricted to subperiods: 1979-1997 (Fig. 6b), and 1997-2012 (Fig. 6c). The relative contributions are calculated by multiplying the changes in *Grad(SST)* and *Mean(SST)* during the given periods by a_1 and a_2, respectively. On average, the regression model captures 98% of the total HCW change for the period 1979-2012 but much less for the shorter subperiods. Both *Mean(SST)* and *Grad(SST)* changes contribute to the HCW change from 1979 to 2012, in different proportion for different reanalyses and simulations. For the subperiods, the regression analysis shows that the observed HC widening from 1979 to 1997 was dominated by an increase in *Mean(SST)*. By contrast, the more recent HC widening from 1997 to 2012, during the global warming hiatus, is dominated by an increase in *Grad(SST)* (i.e., more prevalent La Niña conditions). Because the sensitivity of HCW to *Mean(SST*) is low in AMIP simulations, nearly all of the HCW changes in AMIP simulations is attributable to *Grad(SST)*. In contrast, variations in *Grad(SST)* tend to cancel out when averaged in CMIP5 simulations (because the SST is not observationally constrained so that ENSO events are not in phase with observations or among simulations). Therefore most HCW changes in CMIP5 simulations are attributable to *Mean(SST)*.

4. Discussion and Conclusions

As already noted in previous studies, we found that the Hadley circulation generally widens as surface temperatures increase on large scales, as they do under global warming, and as temperature contrasts between the tropics and midlatitudes decrease, as they do under La Niña (e.g., Lu et al. 2007, 2008; Frierson et al. 2007; Levine and Schneider 2011; Nguyen et al. 2013). One way of interpreting these results at least qualitatively is that the HC terminates at the lowest latitude at which baroclinic eddies become sufficiently deep to reach the upper troposphere, leading to wave activity divergence poleward of that latitude, and thus to upper-tropospheric equatorward flow balancing the resulting angular momentum flux convergence there (Korty and Schneider 2008). Relating the transition latitude to scaling theories for the depth of baroclinic eddies (Held 1978; Schneider and Walker 2006) leads to the expectation that the HC extends to where isentropic slopes first exceeds a critical value

(Korty and Schneider 2008; see also Held 2000; Walker and Schneider 2006; Lu et al. 2007). Because the isentropic slope is a ratio of a meridional temperature gradient and a static stability, the HC is expected to widen as subtropical meridional temperature gradients weaken (like under La Niña) and/or as the static stability increases (like under global warming, because the dry static stability of a moist adiabat increases as the temperature increases). Making these qualitative mechanistic statements quantitative and testing them requires further study.

What we can conclude empirically and quantitatively is that variations in large-scale mean SST (*Mean(SST)*) and in midlatitude-to-tropics SST gradients (*Grad(SST)*) account for about two-thirds of the interannual HCW variations over the years 1979-2012 in 6 reanalyses. They account for a similar portion of interannual HCW variations in 22 AMIP and 11 CMIP5 simulations spanning the years 1979-2008 and 1979-2005, respectively. However, HCW sensitivities to variations in these indices differ substantially among reanalyses and climate models.

Regressing HCW variations on *Mean(SST)* and *Grad(SST)* suggests that the HC widening over the years 1979-1997 is primarily associated with global warming. By contrast, the continued HC widening from 1997 to 2012 is mostly associated with *Grad(SST)* changes consistent with reduced tropics-to-midlatitude temperature contrasts, such as occur under La Niña. More detailed analysis (Fig. 7) reveals that the primary contributor to these *Grad(SST)* changes are elevated midlatitude SST (especially in the Pacific), while tropical SST remain relatively constant. This is consistent with recent theoretical and observational studies that suggest the global warming hiatus is related to increased tropical deep ocean heat uptake, brought about by more prevalent La Niña conditions, while temperatures in the North Pacific are elevated (Meehl et al. 2011; Balmaseda et al. 2013; Kosaka and Xie 2013). However, while these results are not sensitive to the choice of 1997 as the year for subdividing the record, they vary considerably among reanalyses.

The large spread of HCW variations across reanalyses precludes a clear determination of the level of agreement between observed and simulated HCW trends (Quan et al. 2013; Davis and Rosenlof 2012). The ERA-Interim, CFSR, and MERRA reanalyses display similar HCW trends and sensitivity to variations in *Mean(SST)* and *Grad(SST)* as the climate models. The NCEP I, NCEP II, and 20C reanalyses, on the other hand, display significantly larger trends and sensitivity to variations in these indices.

Ozone depletion may also play an important role in the HC widening, in particular at the southern hemisphere (Polvani and Kushner 2002; Polvani et al. 2011). However, as shown here, its contribution to recent widening was likely minor, as the majority of the widening can be accounted for by SST variations, which are at most very weakly affected by ozone depletion.

Acknowledgements

This research was supported by the U.S. National Science Foundation (grant AGS-1049201), and Israeli Science Foundation grant 1537/12. All calculations presented here were performed using GOAT (Geophysical Observation Analysis Tool), a freely available MATLAB based tool for retrieval, analysis and visualization of geophysical data (*http://www.goat-geo.org*).

References

Balmaseda, M. A., K. E. Trenberth, and E. Källén, 2013: Distinctive climate signals in reanalysis of global ocean heat content. *Geophys. Res. Lett.*, **40**, 1754–1759, doi:10.1002/grl.50382.

Ceppi, P., and D. Hartmann, 2012: On the speed of the eddy-driven jet and the width of the Hadley cell in the Southern Hemisphere. *J. Climate*, **26**, 3450–3465, doi:10.1175/JCLI-D-12-00414.1.

Compo, G.P., J.S. Whitaker, P.D. Sardeshmukh, N. Matsui, R.J. Allan, X. Yin, B.E. Gleason, R.S. Vose, G. Rutledge, P. Bessemoulin, S. Brönnimann, M. Brunet, R.I. Crouthamel, A.N. Grant, P.Y. Groisman, P.D. Jones, M. Kruk, A.C. Kruger, G.J. Marshall, M. Maugeri, H.Y. Mok, Ø. Nordli, T.F. Ross, R.M. Trigo, X.L. Wang, S.D. Woodruff, and S.J. Worley, 2011: The Twentieth Century Reanalysis Project. *Quart. J. Roy. Meteor. Soc.*, **137**, 1-28. DOI: 10.1002/qj.776.

Cubasch, U., D. Wuebbles, D. Chen, M. C. Facchini, D. Frame, N. Mahowald and J.-G. Winther, 2013: Introduction. In: *Climate Change 2013: The Physical Science Basis. Contribution of Working Group I to the Fifth Assessment Report of the Intergovernmental Panel on Climate Change* [Stocker, T. F., D. Qin, G.-K. Plattner, M. Tignor, S. K. Allen, J. Boschung, A. Nauels, Y. Xia, V. Bex and P. M. Midgley (eds.)]. Cambridge University Press, Cambridge, United Kingdom and New York, NY, USA, **in press**.

Davis, N. A., and T. Birner, 2013: Seasonal to multidecadal variability of the width of the tropical belt, *J. Geophys. Res. Atmos.*, **118**, 7773–7787, doi:10.1002/jgrd.50610.

Davis, Sean M., and Karen H. Rosenlof, 2012: A Multidiagnostic Intercomparison of

Tropical-Width Time Series Using Reanalyses and Satellite Observations. *J. Climate*, **25**, 1061–1078, doi: http://dx.doi.org/10.1175/JCLI-D-11-00127.1

Dee, D. P., and Coauthors, 2011: The ERA-Interim reanalysis: Configuration and performance of the data assimilation system. *Qart. J. Roy. Meteor. Soc.*, **137**, 553–597, doi:10.1002/qj.828.

Frierson, D. M. W., J. Lu, and G. Chen, 2007: Width of the Hadley cell in simple and comprehensive general circulation models. *Geophys. Res. Lett.*, **34**, L18804, doi:10.1029/2007GL031115.

Hansen, J.E., and S. Lebedeff, 1987: Global trends of measured surface air temperature. *J. Geophys. Res.*, **92**, 13345-13372, doi:10.1029/JD092iD11p13345

Held, I. M., 1978: The vertical scale of an unstable baroclinic wave and its importance for eddy heat flux parameterizations, *J. Atmos. Sci.*, **35**, 572 – 576.

----- , 2000: The general circulation of the atmosphere, paper presented at 2000 Woods Hole Oceanographic Institute Geophysical Fluid Dynamics Program, Woods Hole Oceanographic Institute, Woods Hole, Mass., *http://gfd.whoi.edu/proceedings/2000/PDFvol2000.html*.

Hu, Y., and Q. Fu, 2007: Observed poleward expansion of the Hadley circulation since 1979. *Atmos. Chem. Phys.*, **7**, 5229–5236, doi:10.5194/acp-7-5229-2007.

Johanson, Celeste M., and Qiang Fu, 2009: Hadley Cell Widening: Model Simulations versus Observations. *J. Climate*, **22**, 2713–2725. doi: http://dx.doi.org/10.1175/2008JCLI2620.1

Kalnay, E., and Coauthors, 1996: The NCEP/NCAR 40-year reanalysis project. *Bull. Amer. Meteor. Soc.*, **77**, 437–471, doi:10.1175/1520-0477(1996)077<

0437:TNYRP>2.0.CO;2.

Kanamitsu, M., and Coauthors, 2002: NCEP dynamical seasonal forecast system 2000. *Bull. Amer. Meteor. Soc.*, **83**, 1019–1037.

Kang, Sarah M., Clara Deser, and Lorenzo M. Polvani, 2013: Uncertainty in Climate Change Projections of the Hadley Circulation: The Role of Internal Variability. *J. Climate*, **26**, 7541–7554. doi: http://dx.doi.org/10.1175/JCLI-D-12-00788.1

----- , Jian Lu, 2012: Expansion of the Hadley Cell under Global Warming: Winter versus Summer. J. Climate, 25, 8387–8393. doi: http://dx.doi.org/10.1175/JCLI-D-12-00323.1

Korty, R. L., and T. Schneider, 2008: Extent of Hadley circulations in dry atmospheres. *Geophys. Res. Lett.*, **35**, L23803, doi:10.1029/2008GL035847

Kosaka,Y.and Xie, S-P., 2013:. Recent global-warming hiatus tied to equatorial Pacific surface cooling. *Nature*, **501**,403–407.

Levine, X. J., and T. Schneider, 2011: Response of the Hadley circulation to climate change in an aquaplanet GCM coupled to a simple representation of ocean heat transport. *J. Atmos. Sci.*, **68**, 769–783.

Liu, Z., S. J. Vavrus, F. He, N. Wen, and Y. Zhang, 2005: Re- thinking tropical ocean response to global warming: The enhanced equatorial warming. *J. Climate*, **18**, 4684–4700.

Lu, J., G. A. Vecchi, and T. Reichler, 2007: Expansion of the Hadley cell under global warming. *Geophys. Res. Lett.*, **34**, L06805, doi:10.1029/2006GL028443.

----- , Gang Chen, Dargan M. W. Frierson, 2008: Response of the Zonal Mean Atmospheric Circulation to El Niño versus Global Warming. *J. Climate*, **21**, 5835–

5851. doi: http://dx.doi.org/10.1175/2008JCLI2200.1

Lucas, C., Timbal, B. and Nguyen, H., 2014: The expanding tropics: a critical assessment of the observational and modeling studies. *WIREs Clim. Change,* **5**, 89–112. doi: 10.1002/wcc.251

Meehl, G. A., J. Arblaster, J. Fasullo, A. Hu, and K. Trenberth, 2011: Model- based evidence of deep ocean heat uptake during surface temperature hiatus periods, *Nature. Climate Change*, **1**, 360–364, doi:10.1038/NCLIMATE1229.

Nguyen, H., A. Evans, C. Lucas, I. Smith, B. Timbal, 2013: The Hadley Circulation in Reanalyses: Climatology, Variability, and Change. *J. Climate*, **26**, 3357–3376. doi: http://dx.doi.org/10.1175/JCLI-D-12-00224.1

Polvani, L.M, D.W. Waugh, G.J.P. Correa and S.-W. Son, 2011: Stratospheric ozone depletion: the main driver of 20th Century atmospheric circulation changes in the Southern Hemisphere. *J. Climate*, **24**, 795-812, doi:10.1175/2010JCLI3772.1

----- , and P.J. Kushner, 2002: Tropospheric response to stratospheric perturbations in a relatively simple general circulation model. *Geophys. Res. Lett.*, **29**, doi:10.129/2001GL014284

Quan, X., M. Hoerling, J. Perlwitz, H. Diaz, and T. Xu, 2013: How fast are the tropics expanding?. *J. Climate.* doi:10.1175/JCLI-D-13-00287.1, in press

Rienecker, Michele M., and Coauthors, 2011: MERRA: NASA's Modern-Era Retrospective Analysis for Research and Applications. *J. Climate*, **24**, 3624–3648. doi: http://dx.doi.org/10.1175/JCLI-D-11-00015.1

Saha, Suranjana, and Coauthors, 2010: The NCEP Climate Forecast System Reanalysis. *Bull. Amer. Meteor. Soc.*, **91**, 1015–1057. doi:

http://dx.doi.org/10.1175/2010BAMS3001.1

Schneider, T., and C. C. Walker, 2006: Self-organization of atmospheric macroturbulence into critical states of weak nonlinear eddy-eddy interactions. *J. Atmos. Sci.*, **63**, 1569-1586.

Seager, Richard, Nili Harnik, Yochanan Kushnir, Walter Robinson, Jennifer Miller, 2003: Mechanisms of Hemispherically Symmetric Climate Variability*. *J. Climate*, **16**, 2960–2978.

Seidel, D. J., and W. J. Randel, 2007: Recent widening of the tropical belt: Evidence from tropopause observations, *J. Geophys. Res.*, **112**, D20113, doi:10.1029/2007JD008861.

Smith, T.M., R.W. Reynolds, Thomas C. Peterson, and Jay Lawrimore, 2008: Improvements to NOAA's Historical Merged Land-Ocean Surface Temperature Analysis (1880-2006). *J. Climate*, **21**, 2283-2296.

Walker, C. C., and T. Schneider, 2006: Eddy influences on Hadley circulations: Simulations with an idealized GCM. *J. Atmos. Sci.*, **63**, 3333–3350.

Captions

Table 1. Reanalysis datasets and AMIP and CMIP5 climate simulations used in this study. Resolutions are given as number of latitude x longitude grid points or spectral truncation, times the number of vertical levels. In the models names, LR and MR refer to low and medium resolutions, (A), (H), and (A/H) refer to AMIP, historical, and both AMIP and historical climate simulations.

Figure 1. EOFs and principal components (PC) of SST variations, and SST variations associated with ENSO. (a) First (solid red) and second (solid blue) EOFs of zonal- and annual-mean SST variations, and difference between composite El Niño and La Niña conditions (orange dashed) for the years 1979-2012 (ERSST v3b). Here, El Niño (La Niña) conditions are defined as ONI values greater (smaller) than 0.5 (-0.5). The normalized EOFs are multiplied by a factor of 2 K to match approximately the amplitude of the SST composite of typical El Niño minus La Niña SST conditions. (b) Principal component time series associated with the first and second EOF (solid red and blue), and ONI index (orange dashed).

Figure 2. Top: time series of *Mean(SST)* (solid, green) and global-mean (land-ocean) surface temperature anomaly averaged between ±45° latitude (dashed, magenta, GISTEMP) for the years 1979-2012. The *Mean(SST)* trends (solid gray) with 95% confidence bounds (shading) are shown for the periods 1979-1997 (0.1 ±0.054 K/decade), and 1997-2012 (dark gray, 0.025 ±0.068 K/decade). The mean value of *Mean(SST)* is 296.1 K (23°C). **Bottom:** time series of *Grad(SST)* (solid blue, left vertical axis), and ONI (dashed orange, multiplied by -1, right vertical axis). The (Pearson) correlation coefficient between ONI and *Grad(SST)* is -0.8. The *Grad(SST)*

trends (solid gray) with 95% confidence bounds (shading) are shown for the periods 1979-1997 (0 ±0.12 K/decade), and 1997-2012 (0.086 ±0.18 K/decade). The mean value of *Grad(SST)* is -7.8 K.

Figure 3. Top: time series (1979-2011) of the annually averaged Hadley circulation width (HCW) for the 6 reanalyses. Thick black and gray lines show ensemble means and linear trends (0.93° ±0.43°/decade), respectively**. Bottom:** time series of the HC extent with linear trend in the northern hemisphere (0.51° ±0.33°/decade) and southern hemisphere separately (-0.42° ±0.21°/decade) separately. The vertical axis is truncated for compactness. The spread of HCW across models has a standard deviation of 0.2°, which increases with time at a statistically significant ($p<0.05$) rate of 30% per decade.

Figure 4. Trends in poleward shift of HC terminus (°/decade) in the southern hemisphere (left) and northern hemisphere (right) during 1979-2005 for reanalyses (orange triangles), for AMIP simulations (blue crosses), and for CMIP5 simulations (green dots). Error bars show Studentized 95% confidence bounds. Ensemble means are shown as the respective symbol without error bars.

Figure 5. HCW sensitivity to variations in *Mean(SST)* (left) and *Grad(SST)* (right), for reanalyses (orange triangles), AMIP simulations (blue crosses), and CMIP5 simulations (green dots). Error bars show Studentized 95% confidence bounds. Ensemble means are shown as the respective symbol without error bars. The periods used for the calculation of the sensitivities are 1979-2012, 1979-2008, and 1979-2005

for reanalyses, AMIP simulations, and CMIP5 simulations, respectively (with the exception of 1979-2011 for the 20C Reanalysis).

Figure 6. Mean change in HCW (orange) and the respective change due to variations in *Mean(SST)* (green) and *Grad(SST)* (blue) in the 6 reanalyses, and in the AMIP and CMIP5 simulations (ensemble means). (a) Changes over 1979-2012 for reanalyses (1979-2011 for 20C Rean.), over 1979-2008 for AMIP simulations, and over 1979-2005 for CMIP5 simulations. (b) As for (a), but changes restricted to 1979-1997. (c) As for (a), but changes restricted to 1997-2012 for reanalyses (1997-2011 for 20C Rean.), to 1997-2008 for AMIP simulations, and to 1997-2005 for CMIP5 simulations. The mean Studentized 95% confidence error bounds are (a) ±1.4°, (b) ±1.7°, and (c) ±2°.

Figure 7. Time series of the zonally and annually averaged SST anomaly (ERSST) during 1979-2012 in the latitude bands 20°N-45°N (top), 20°S-20°N (middle), and 45°S-20°S (bottom).

Figures

Reanalysis	***Source and Description***	***Resolution***
NCEP-I	National Center for Environmental Prediction–National Center for Atmospheric Research (NCEP–NCAR) Global Reanalysis I (Kalnay et al. 1996)	T62×28
NCEP-II	NCEP/Department of Energy Global Reanalysis II (Kanamitsu et al. 2002)	T62×28
ERA-Interim	European Center for Medium-Range Weather Forecasts (ECMWF) Interim Reanalysis (Dee et al. 2011)	T225×60
MERRA	NASA Modern Era Retrospective-Analysis for Research and Applications (Rienecker et al. 2011)	720×270×72
20th Cent. Rean.	National Oceanic and Atmospheric Administration (NOAA)-Cooperative Institute for Research in Environmental Sciences Twentieth-Century Reanalysis VII (Compo et al. 2011)	T62×28
CFSR	NCEP Climate Forecast System Reanalysis (Saha et al. 2010)	T382×64
Climate Model		
BCC-CSM1.1(A/H)	Beijing Climate Center Climate System Model, ver. 1.1	T42×26
BNU-ESM(A)	College of Global Change and Earth System Science, Beijing Normal University	T42×26
CanAM4(A)	Fourth generation Canadian Atmospheric Climate Model	T63×35
CanCM4(H)	Fourth generation Canadian Coupled Global Climate Model	T63×35
CanESM2(H)	Second generation Canadian Earth System Model	T63×35
CCSM4(A/H)	Community Climate System Model, version 4.0	288×192×26
CMCC-CM(A)	Euro-Mediterranean Center for Climate Change	T159×31
CSIRO-Mk3.6(A)	Commonwealth Scientific and Industrial Research Organization Mark, ver. 3.6.0	T63×18
EC-EARTH(A)	EC-Earth consortium Earth System Model	T159×62
FGOALS-G2.0(A)	Flexible Global Ocean–Atmosphere–Land System Model, gridpoint, ver. 2	T42×26
GFDL-CM2p1(H)	Geophysical Fluid Dynamics Laboratory (GFDL) Climate Model 2.1	144×90×24
GFDL-CM3(A/H)	GFDL Climate Model, ver. 3	144×90×48
GFDL-ESM2G(H)	GFDL Earth System Model with GOLD 3 ocean component	144×90×24
GFDL-ESM2M(H)	GFDL Earth System Model with MOM4 ocean component	144×90×24
GFDL-HIRAM-180(A)	GFDL High Resolution Atmospheric Model	576×360×17
GFDL-HIRAM-360(A)	GFDL High Resolution Atmospheric Model	1152×720×17
GISS-E2-H-CC(H)	Goddard Institute for Space Studies (GISS) Model E, coupled with HYCOM ocean model	180×73×40
GISS-E2-R(A/H)	GISS Model E, coupled with Russell ocean model	144×90×40
GISS-E2-R-CC(H)	GISS Model E, coupled with Russell ocean model	180×73×40
HadGEM2(A)	Hadley Centre Global Environmental Model, ver. 2	192×145×40
INMCM4(A)	Institute of Numerical Mathematics Coupled Model, ver. 4	180×120×21
IPSL-CM5A-LR(A)	L'Institut Pierre-Simon Laplace Coupled Model, ver. 5A	96×96×39
IPSL-CM5A-MR(A)	L'Institut Pierre-Simon Laplace Coupled Model, ver. 5A	144×143×39
IPSL-CM5B-LR(A)	L'Institut Pierre-Simon Laplace Coupled Model, ver. 5B	96×96×39
MPI-ESM-LR(A)	Max Planck Institute Earth System Model	T63×47
MPI-ESM-MR(A)	Max Planck Institute Earth System Model	T63×95
MRI-AGCM3.2H(A)	Meteorological Research Institute of Japan, Atmospheric GCM	T319×64
MRI-CGCM3(A)	Meteorological Research Institute of Japan, Coupled GCM	T159×48
NorESM1-M(A)	Norwegian Earth System Model, ver. 1	144×96×26

Table 1. Reanalysis datasets and AMIP and CMIP5 climate simulations used in this study. Resolutions are given as number of latitude x longitude grid points or spectral truncation, times the number of vertical levels. In the models names, LR and MR refer to low and medium resolutions, (A), (H), and (A/H) refer to AMIP, historical, and both AMIP and historical climate simulations.

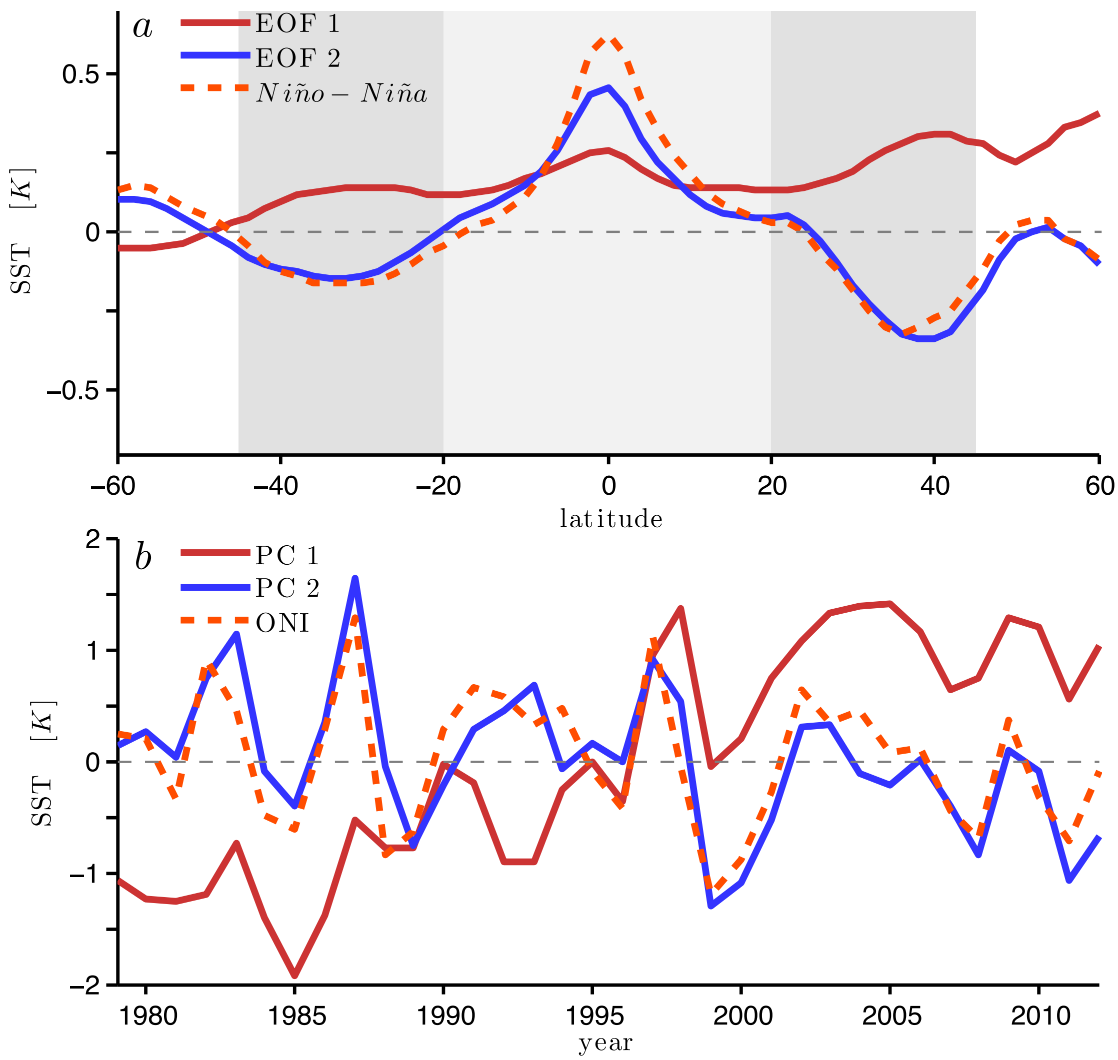

Figure 1. EOFs and principal components (PC) of SST variations, and SST variations associated with ENSO. (a) First (solid red) and second (solid blue) EOFs of zonal- and annual-mean SST variations, and difference between composite El Niño and La Niña conditions (orange dashed) for the years 1979-2012 (ERSST v3b). Here, El Niño (La Niña) conditions are defined as ONI values greater (smaller) than 0.5 (-0.5). The normalized EOFs are multiplied by a factor of 2 K to match approximately the amplitude of the SST composite of typical El Niño minus La Niña SST conditions. (b)

Principal component time series associated with the first and second EOF (solid red and blue), and ONI index (orange dashed).

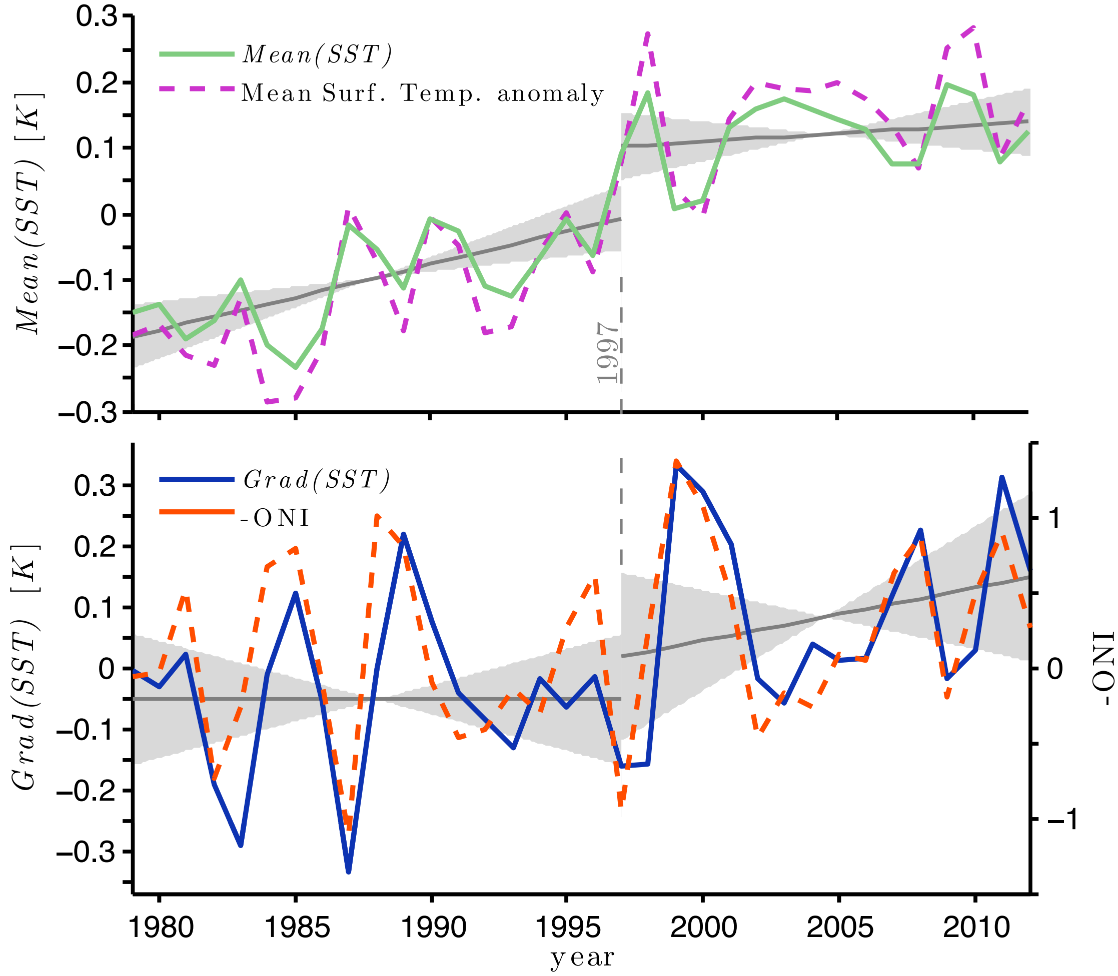

Figure 2. Top: time series of *Mean(SST)* (solid, green) and global-mean (land-ocean) surface temperature anomaly averaged between ±45° latitude (dashed, magenta, GISTEMP) for the years 1979-2012. The *Mean(SST)* trends (solid gray) with 95% confidence bounds (shading) are shown for the periods 1979-1997 (0.1 ±0.054 K/decade), and 1997-2012 (dark gray, 0.025 ±0.068 K/decade). The mean value of *Mean(SST)* is 296.1 K (23°C). **Bottom:** time series of *Grad(SST)* (solid blue, left vertical axis), and ONI (dashed orange, multiplied by -1, right vertical axis). The (Pearson) correlation coefficient between ONI and *Grad(SST)* is -0.8. The *Grad(SST)* trends (solid gray) with 95% confidence bounds (shading) are shown for the periods

1979-1997 (0 ±0.12 K/decade), and 1997-2012 (0.086 ±0.18 K/decade). The mean value of *Grad(SST)* is -7.8 K.

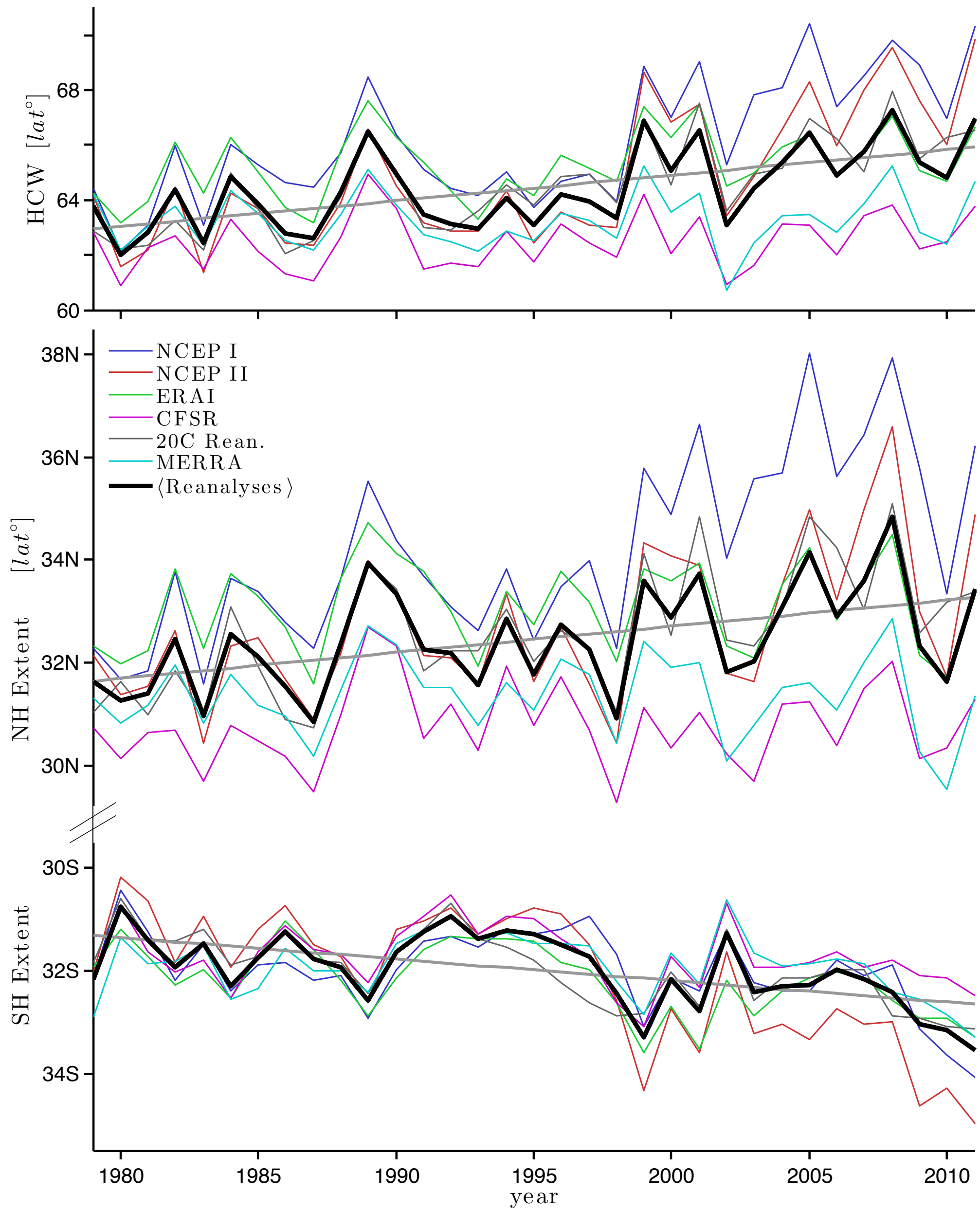

Figure 3. Top: time series (1979-2011) of the annually averaged Hadley circulation width (HCW) for the 6 reanalyses. Thick black and gray lines show ensemble means and linear trends (0.93° ±0.43°/decade), respectively**. Bottom:** time series of the HC

extent with linear trend in the northern hemisphere (0.51° ±0.33°/decade) and southern hemisphere separately (-0.42° ±0.21°/decade) separately. The vertical axis is truncated for compactness. The spread of HCW across models has a standard deviation of 0.2°, which increases with time at a statistically significant ($p<0.05$) rate of 30% per decade.

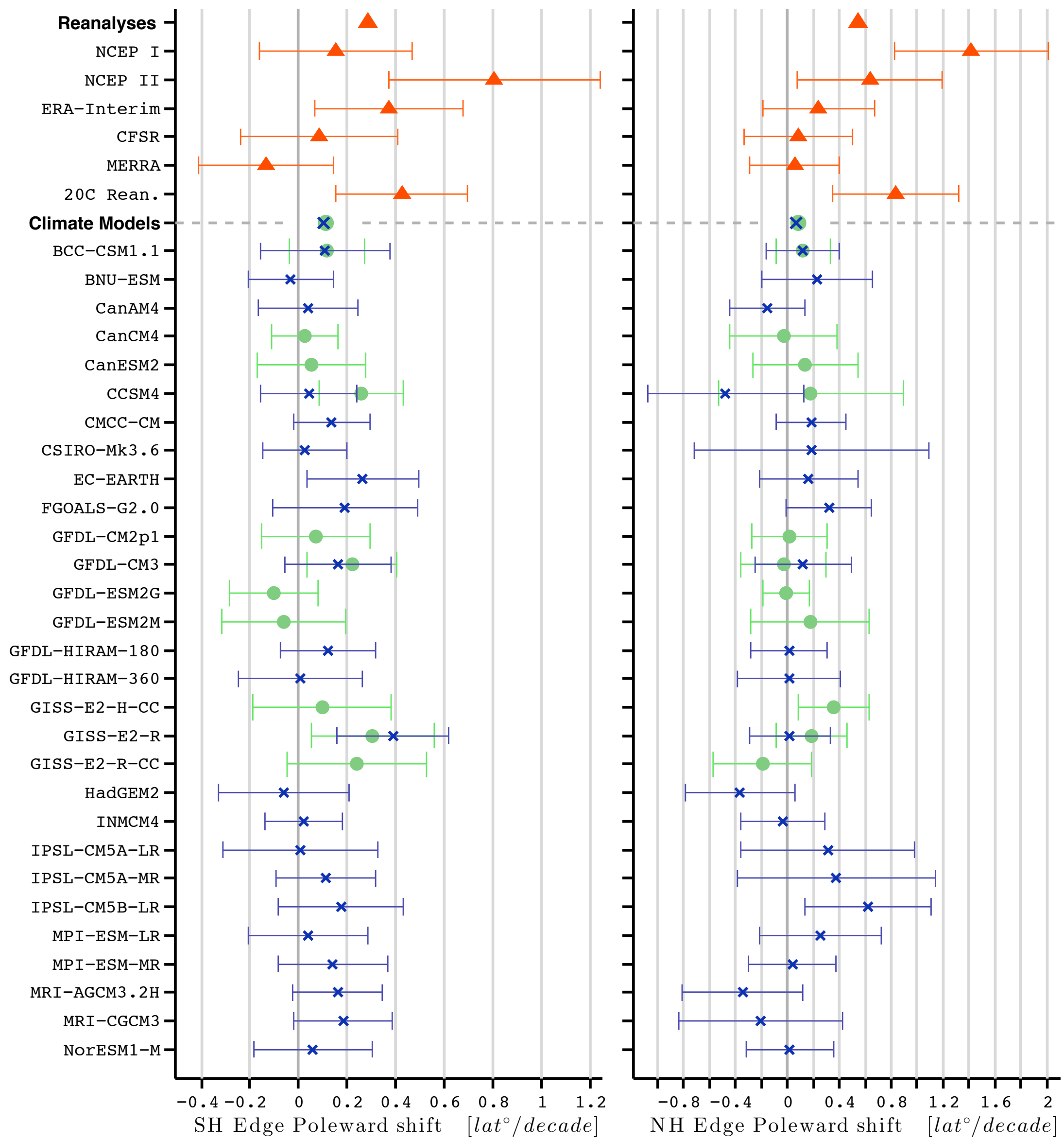

Figure 4. Trends in poleward shift of HC terminus (°/decade) in the southern hemisphere (left) and northern hemisphere (right) during 1979-2005 for reanalyses

(orange triangles), for AMIP simulations (blue crosses), and for CMIP5 simulations (green dots). Error bars show Studentized 95% confidence bounds. Ensemble means are shown as the respective symbol without error bars.

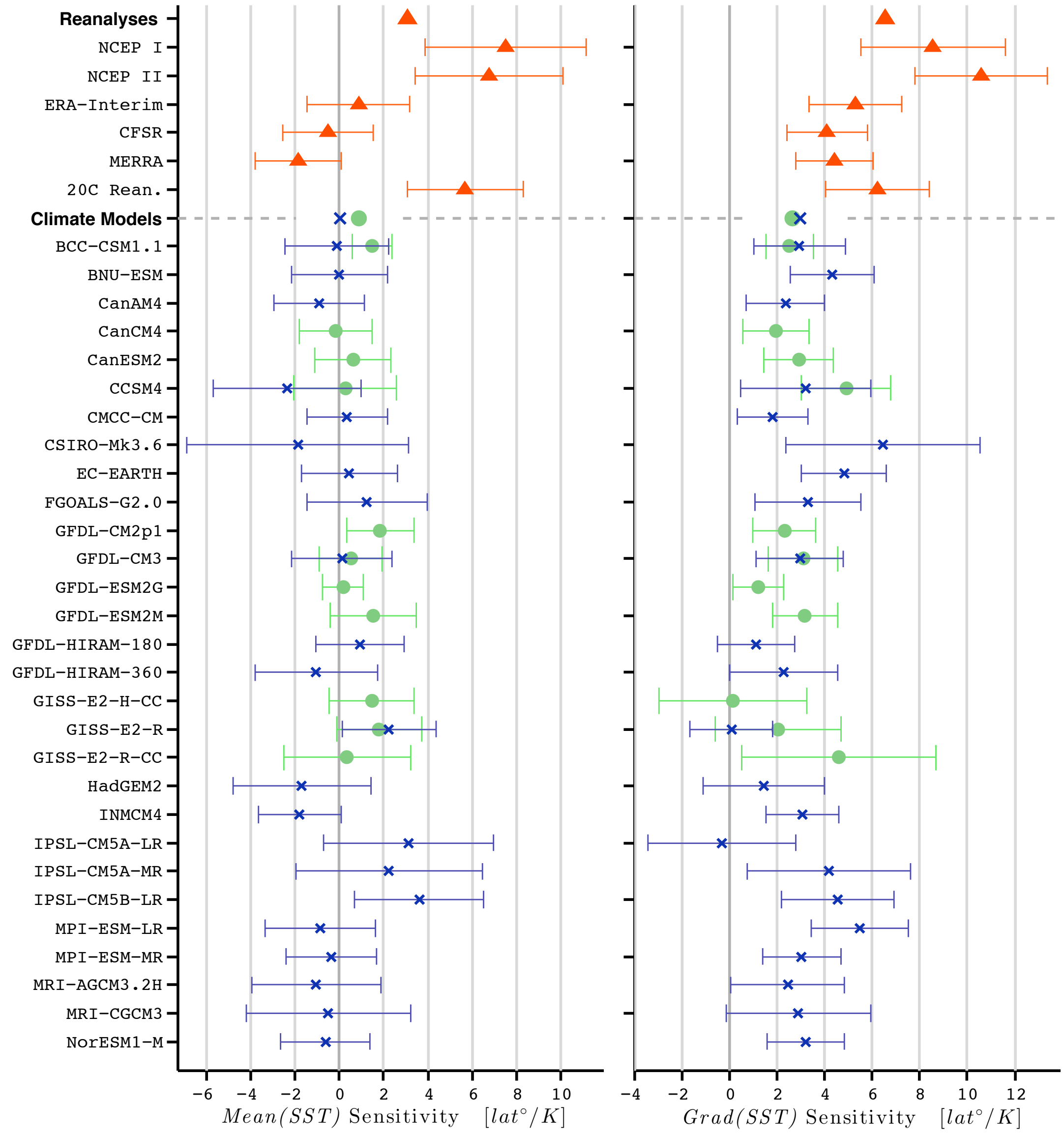

Figure 5. HCW sensitivity to variations in *Mean(SST)* (left) and *Grad(SST)* (right), for reanalyses (orange triangles), AMIP simulations (blue crosses), and CMIP5 simulations (green dots). Error bars show Studentized 95% confidence bounds. Ensemble means are shown as the respective symbol without error bars. The periods used for the calculation of the sensitivities are 1979-2012, 1979-2008, and 1979-2005 for reanalyses, AMIP simulations, and CMIP5 simulations, respectively (with the exception of 1979-2011 for the 20C Reanalysis).

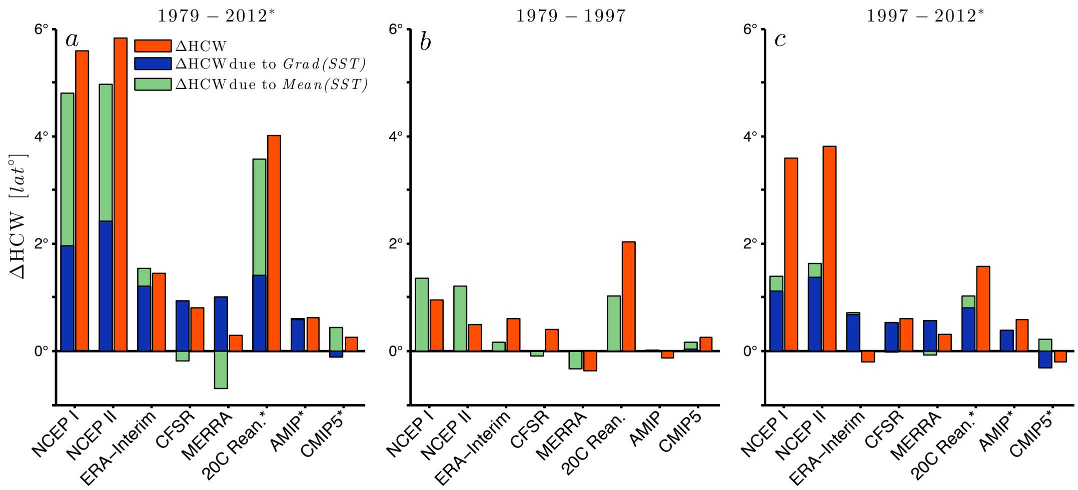

Figure 6. Mean change in HCW (orange) and the respective change due to variations in *Mean(SST)* (green) and *Grad(SST)* (blue) in the 6 reanalyses, and in the AMIP and CMIP5 simulations (ensemble means). (a) Changes over 1979-2012 for reanalyses (1979-2011 for 20C Rean.), over 1979-2008 for AMIP simulations, and over 1979-2005 for CMIP5 simulations. (b) As for (a), but changes restricted to 1979-1997. (c) As for (a), but changes restricted to 1997-2012 for reanalyses (1997-2011 for 20C Rean.), to 1997-2008 for AMIP simulations, and to 1997-2005 for CMIP5 simulations. The mean Studentized 95% confidence error bounds are (a) ±1.4°, (b) ±1.7°, and (c) ±2°.

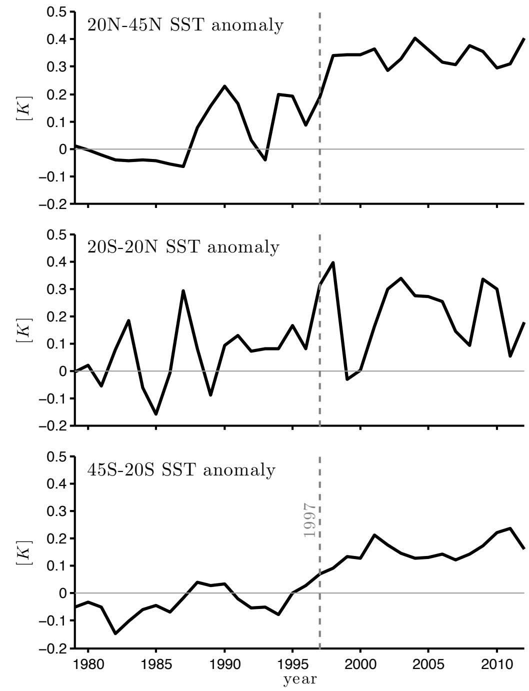

Figure 7. Time series of the zonally and annually averaged SST anomaly (ERSST) during 1979-2012 in the latitude bands 20°N-45°N (top), 20°S-20°N (middle), and 45°S-20°S (bottom).